

Ultralong Spin Lifetime in Light Alkali Atom Doped Graphene

B. G. Márkus,^{†,‡} P. Szirmai,[‡] K. F. Edelthammer,[¶] P. Eckerlein,[¶]
 A. Hirsch,[¶] F. Hauke,[¶] N. M. Nemes,[§] J. C. Chacón-Torres,^{||} B. Náfrádi,[‡]
 L. Forró,[‡] T. Pichler,[⊥] and F. Simon^{*,†,‡}

[†]*Department of Physics, Budapest University of Technology and Economics and MTA-BME Lendület Spintronics Research Group (PROSPIN), PO Box 91, H-1521 Budapest, Hungary*

[‡]*Laboratory of Physics of Complex Matter, École Polytechnique Fédérale de Lausanne, Lausanne CH-1015, Switzerland*

[¶]*Department of Chemistry and Pharmacy and Institute of Advanced Materials and Processes (ZMP), University of Erlangen-Nürnberg, Nikolaus-Fiebiger-Strasse 10, 91058 Erlangen, Germany*

[§]*GFMC, Unidad Asociada ICMM-CSIC "Laboratorio de Heteroestructuras con Aplicacion en Espintronica", Departamento de Fisica de Materiales Universidad Complutense de Madrid, 28040 Madrid, Spain*

^{||}*Universidad UTE, Facultad de Ciencias, Ingeniería y Construcción, 170147 Quito, Ecuador and Yachay Tech University, School of Physical Sciences and Nanotechnology, 100119 Urcuquí, Ecuador*

[⊥]*Faculty of Physics, University of Vienna, Strudlhofgasse 4., Vienna, A-1090, Austria*

E-mail: f.simon@eik.bme.hu

ABSTRACT

Today's great challenges of energy and informational technologies are addressed with a singular compound, the Li and Na doped few layer graphene. All what is impossible for graphite (homogeneous and high level Na doping), and unstable for single layer graphene, works very well for this structure. The transformation of the Raman G line to a Fano lineshape and the emergence of strong, metallic-like electron spin resonance (ESR) modes, attest the high level of graphene doping in liquid ammonia for both kinds of alkali atoms. The spin-relaxation time in our materials, deduced from the ESR line-width, is 6-8 ns, which is comparable to the longest values found in spin-transport experiments on ultrahigh mobility graphene flakes. This could qualify our material as promising candidate in spintronics devices. On the other hand, the successful sodium doping, this being a highly abundant metal, could be an encouraging alternative to lithium batteries.

KEYWORDS:

few-layer graphene, alkali atom doping, Raman spectroscopy, electron spin lifetime, electron spin resonance

Charge state in various forms of carbon can be conveniently controlled using alkali atom doping methods. It led to applications in *e.g.* energy storage¹ and to the discovery of compelling correlated phases such as *e.g.* superconductivity (with $T_c = 11.5$ K in CaC_6 Ref.^{2,3} and $T_c = 28$ K in Rb_3C_{60} Ref.⁴), spin density waves in fullerenes,⁵ and the Tomonaga–Luttinger to Fermi liquid crossover in single-wall carbon nanotubes.^{6,7}

Control over the number of free electrons in carbon could be also exploited in spintronics,^{8–10} *i.e.* when using the electron spin as an information carrier and storage unit. Doping-induced metallic carbon has the smallest spin-orbit coupling besides metallic Li and Be, which is expected to result in ultralong spin lifetime, τ_s ; a prerequisite for spintronics. Graphene arose as a promising candidate for spintronics purposes due to the predicted long τ_s , its actual value is controversial according to spin transport studies^{11–16} and it ranges from 100 ps¹¹ up to 12 ns^{12,15,16} with theoretical hints that the short lifetime originates from extrinsic effects.¹⁷ Doping graphene with light alkali atoms would enable the accurate determination τ_s for the itinerant electrons by spin spectroscopy, *i.e.* electron spin resonance (ESR).^{18,19} Light alkali atoms have a small spin-orbit coupling^{20,21} thus the intrinsic spin lifetime in graphene is expected to be observed with this approach.

Conventional alkali doping of carbon proceeds in the so-called vapor phase which works well for heavier alkali atoms with a lower melting point (K, Rb, and Cs):²² the alkali atoms are heated together with the desired form of carbon (graphite, graphene, nanotubes, or fullerene). For Li and Ca doping, graphite doping was achieved by immersing the sample into molten Li or Li/Ca mixtures² with temperatures up to 350 °C. This relatively high temperature is dictated by the melting point and is due to the slow kinetics of the diffusion process but the reaction has a small temperature window due to formation of alkali carbides around 450 °C. This method can only be formed for bulky sample (*e.g.* for a piece of HOPG or graphite single crystal) which can be inserted and removed from the molten metal.

Alkali atom doping of graphene is also intensively studied.^{23–29} Achieving controllable and high level doping would be particularly important

for chemically exfoliated graphene, which is the bulk form of graphene, *e.g.* for energy storage purposes.^{30–32} Especially Na doped graphene is an important candidate to replace conventional Li-ion batteries due to the low cost and high abundance of sodium.^{33–36}

However, Na is somewhat of an outlier among the alkali metals as it does not intercalate graphite under ambient pressure except for a very low stoichiometry of NaC_{64} ^{37–41} as compared to *e.g.* LiC_6 and KC_8 . Successful Na doping was reported for graphene, prepared by a solvothermal synthesis by the Choucair method,⁴² either using electrochemical doping⁴³ or when the material was synthesized from Na containing precursors.⁴⁴ However, solvothermal-derived graphene is known to have a relatively large defect concentration as well as a limited flake size, it is thus intriguing whether Na doping could be achieved for a high quality and high area mono or few-layer graphene.

As mentioned, doping with light alkali atoms cannot be performed with the vapor phase method. An alternative doping route uses solvents, such as liquid ammonia and organic solvents (*e.g.* tetrahydrofuran (THF)⁴⁵ or 2-methyltetrahydrofuran (2-MeTHF) and 2,5-dimethyltetrahydrofuran (diMeTHF)^{46,47}). These are known to dissolve well the alkali and some alkaline-earth elements. Then, the reaction between the alkali atoms and the carbon material proceeds in the solution at moderate temperatures and with a high efficiency due to the large reaction surface. This procedure was used to obtain highly doped fullerenes^{48–53} and carbon nanotubes (nanotubides).⁵⁴ This route is promising for doping graphene with light alkali atoms and it could address the value of spin lifetime of itinerant electrons and whether Na can differentiate between mono and few-layer graphene, as the latter is known to be inevitably present in chemically exfoliated graphene.⁵⁵

Here, we report synthesis of Li and Na doped few-layer graphene (FLG) using liquid ammonia. The FLG material was prepared by chemical exfoliation. Raman spectroscopy, conductivity, and electron spin resonance studies indicate a successful doping. The strongly Fano-like Raman lineshapes evidence a sizable electron-phonon coupling. However, neither SQUID mag-

netometry nor conductivity measurements gave evidence for a superconducting phase down to 2 K. The spin-relaxation lifetime of conduction electrons is in excess of 7 ns which represents an ultralong value especially for chemically exfoliated graphene. We argue that Na dopes selectively monolayer graphene as a few-layer graphene resembles graphite for which Na doping is known to be impossible.

RESULTS AND DISCUSSION

Few-layer graphene (FLG) samples were doped with lithium and sodium in liquid ammonia with the setup shown in Fig. 1a. We previously demonstrated that the starting material mainly consists of graphene flakes with 5 or less layers with a log-normal distribution centered around 3 layers.⁵⁵ Photographs of the samples are presented in Fig. 1b. and c. A characteristic color change was observed to the black FLG material upon doping, which is a fingerprint of charge transfer from the alkali atoms toward the carbon, as seen before for graphite intercalation compounds^{22,56} and graphene.^{23,24,55} In case of lithium, both yellow-brownish and bluish spots are present, which attests a successful doping of the material. For sodium, only bluish areas are observable, which hints at lighter, yet successful doping. For intercalated graphite, yellow color is the signature of the highest level of doping (also referred to as stage-I compounds), whereas blue color is a signature of a lower level of doping.²²

The most striking observation of this synthesis process is the presence of *any* color change to the Na doped FLG sample. Na is known to intercalate (or dope) graphite to a very low level such as NaC_{64} ³⁷⁻⁴⁰ which has the same color as graphite. In fact, higher level of Na doping can only be achieved with an ultra high pressure synthesis method⁵⁷ but the resulting material is unstable at ambient pressure. It has long been intriguing why Na does not effectively dope graphite. Graphite intercalation compounds possess a long-range ordered structure for the alkali atoms and also for the graphene layers which are adjacent to layers of alkali atoms. Recent *ab initio* calculations⁴¹ hint at a delicate interplay between the

alkali ion induced structural deformation (and the corresponding weakening in the van der Waals interaction between graphene layers), the covalent (for Li) *versus* ionic (for Na) interaction which makes the formation of Na intercalated graphite thermodynamically unfavored. In contrast, sodium can effectively dope fullerenes up to Na_4C_{60} ,⁵⁸⁻⁶⁰ where the voids between the fullerene balls can be conveniently filled thus the deformation energy of the van der Waals molecular crystal is smaller and is compensated by the energy gain during the electron charge transfer. Therefore it is expected that Na could dope monolayer graphene where the energy loss due to deformation is also absent.

Given the surprising result of a successful and relatively high level of Na doping of the few layer graphene sample, we performed Raman spectroscopy on the synthesized materials as it is a sensitive probe of the charge transfer toward the carbonaceous material. Raman spectra recorded at 514.5 nm wavelength of the materials are presented in Fig. 2. Raman spectrum of the pristine material displays the usual D (1358 cm^{-1}), G (1580 cm^{-1}), and 2D (2710 cm^{-1}) bands and it reproduces the earlier reports on similar samples.⁶¹

The lithium doped FLG sample shows a broad and intensive Fano-shaped line (also referred as Breit-Wigner-Fano or BWF lineshape)^{62,63} at 1507 cm^{-1} , which dominates the spectrum. The D and 2D modes are barely visible and the latter is extremely broadened. The Fano line is downshifted and flattened compared to the original G mode, as expected upon heavy doping. Compared to the Raman spectrum of LiC_6 GIC, the observed peak is relatively close to its E_{2g1} mode at 1546 cm^{-1} . The doped samples are in a quartz tube which explains the origin of the Raman line denoted by an asterisk.

We also present Raman data for two Na doped samples, one denoted as heavily, the other as moderately doped. The heavy doping notation refers to the highest achievable doping level whereas the moderate doping is representative for a sample prepared with a smaller amount of alkali dopants. Both types of sodium doped samples present a Fano line at around 1572 cm^{-1} and a symmetric Lorentzian peak at $1600 - 1602\text{ cm}^{-1}$. The Fano peak at the lower Raman shift confirms the presence of highly intercalated flakes in agreement

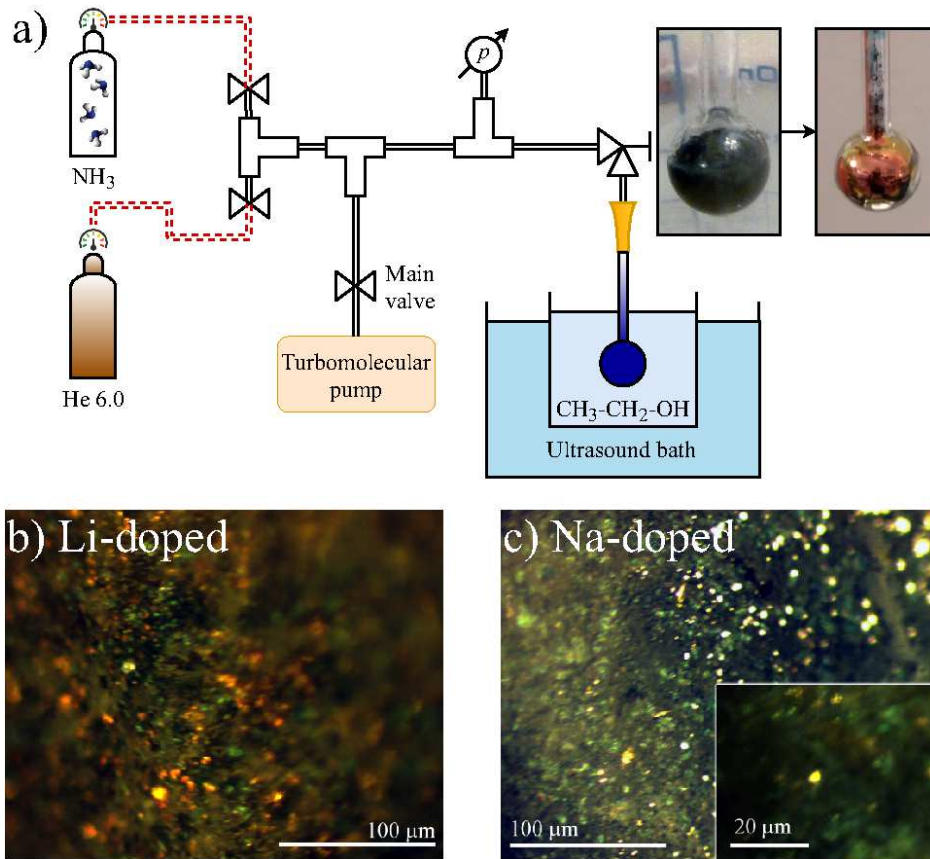


Figure 1: a) Schematics of the doping setup connected to a vacuum line with gas inlets. The alkali-ammonia solution (blue bubble) is kept around $-40\text{ }^{\circ}\text{C}$ using an ethanol bath. A bath sonicator assists the doping and it surrounds the ethanol container. Inset shows the photograph of the solution at the beginning and at the end of the process. b) and c) Microscope images of the final materials. Note that Li doping results in bright, yellow-brownish and bluish flakes, while upon Na doping only bluish areas are present. Inset in c) shows a smaller area of the sodium doped sample shot with a $50\times$ objective to emphasize the presence of bluish areas.

with the above mentioned surprising microscopic observation, *i.e.* that significant charge transfer is observed in the Na doped samples. The Fano lineshape in alkali-metal intercalation compounds with graphite only occurs when a stage-I compound is reached, that means when each graphene layer is surrounded from both sides by an alkali atom layer.⁶⁴ The observation of this asymmetric mode in the Na doped sample provides a direct proof for the existence of Na doped monolayer graphene. The symmetric peak at higher Raman shifts (denoted by G) is associated with weakly charged or incompletely intercalated flakes.⁴⁰ The 2D mode is very broad in all samples as expected for a high level of doping.^{56,64}

In general, the Fano lineshape is the result of quantum interference between the zone-center

phonons and the electronic transitions^{62,63} thus it is an important benchmark of a significant charge transfer in carbonaceous materials including fullerides,⁶⁵ carbon nanotubes (nanotubides),⁶⁶ graphite,⁶⁷ and graphene (graphenides).^{23,24,27}

Additional information about the electronic structure, the level of charge transfer, and the magnitude and sign of the electron-phonon coupling can be obtained from the details of the Fano lineshape. According to Refs.,^{62,63} the lineshape reads as a function of the Raman shift energy, $\hbar\omega$:

$$I(\omega) = I_0 \frac{(q + \bar{\epsilon})^2}{1 + \bar{\epsilon}^2} + A, \quad (1)$$

where q is the Fano asymmetry lineshape parameter, $\bar{\epsilon} = \frac{\omega - \omega_0 - \Delta}{\Gamma/2}$ and A is an offset parameter. Herein $\hbar\omega_0$ is the vibrational energy of the unper-

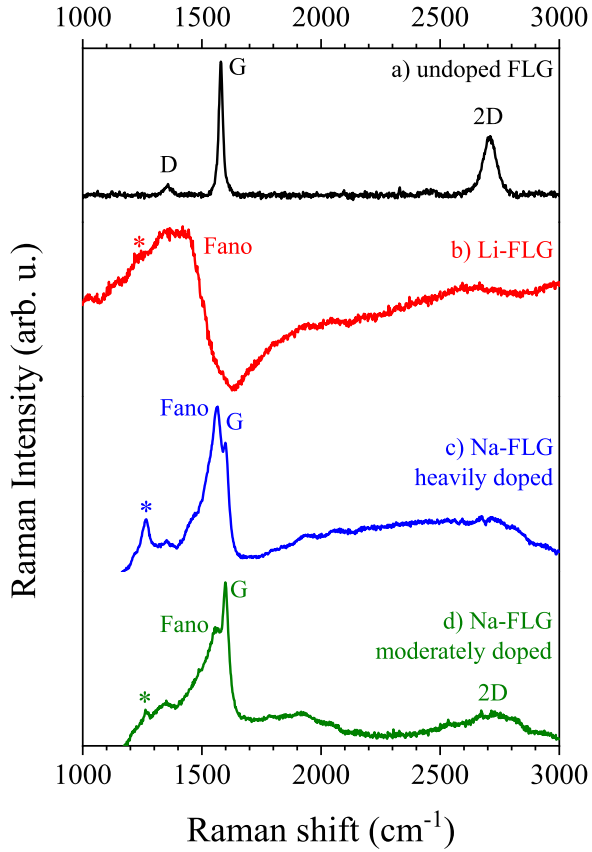


Figure 2: Raman spectra taken at 514.5 nm wavelength. a) Undoped FLG shows the usual D, G and 2D modes. b) A broad and intensive Fano line at 1510 cm^{-1} dominates the spectrum in the lithium doped FLG sample; the D and 2D modes are barely visible and the latter is extremely broadened. c)-d) Sodium doped samples also display a Fano line at 1566 cm^{-1} and a symmetric peak at 1600 cm^{-1} . The latter is denoted by G and is associated with weakly charged graphene flakes. Asterisk denotes a peak from the quartz sample holder.

turbed phonon, $\hbar\Delta$ is the interaction induced shift of the phonon energy and $\hbar\Gamma$ is the broadening parameter due to the interaction. In general Γ and Δ increases with the strength of the electron-phonon coupling however q is inversely proportional to it, $q = \pm\infty$ represents the non-interacting limit and $q \rightarrow 0$ is the limit of strong electron-phonon interaction.

We found $q = -1.03$ for the Li doped FLG and $q = -2.64$ and $q = -3.17$ for the heavily and moderately Na doped FLG samples, respec-

tively (details of the lineshape analysis are provided in the Supplementary Information). These figures have to be compared with $q = -1.09$ found for the graphite intercalation compounds⁵⁶ LiC_6 , KC_8 , and CaC_6 , of which the latter is a superconductor with $T_c = 11.5 \text{ K}$ (Ref.⁶⁸).

The significant charge transfer and the sizable electron-phonon coupling in the Li doped FLG motivated us to search for traces of superconductivity for both the Li and Na doped materials. However, SQUID magnetometry in a zero field cooled condition and using a 10 Oe of sensing field, while warming up the samples from 2 K, did not reveal any traces of superconductivity.

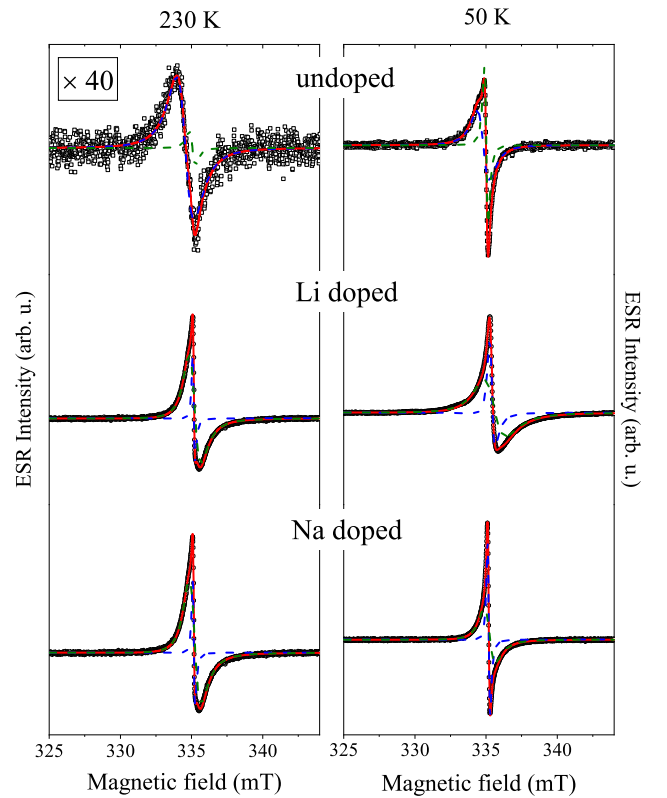


Figure 3: ESR spectra of the undoped, Li and Na doped FLG samples at 230 K and 50 K. Open symbols are the measured data, the fitted curve is represented with a continuous red line. Blue and green curves are the decomposition to the two components present for each sample. The two lines are fully symmetric in the undoped material, whereas both components are asymmetric in the doped ones, indicating a metallic sample. Note the zoomed vertical scale for the undoped material.

Electron spin resonance spectroscopy⁶⁹ can provide a great deal of information about the electrons

in a material, including localized electron spins, which are related to defects or dangling bonds, and also about delocalized, *i.e.* conduction electron species. Fig. 3. presents the ESR spectra of the undoped and Li, Na doped FLG samples at 230 K and 50 K. In each cases, the observed lineshape can be decomposed into two separate lines. In the undoped material, the lines are completely symmetric and thus can be fitted with derivative Lorentzians. The origin of these lines is most probably dangling bonds or lattice defects, which give rise to a paramagnetic signal. The presence of such lines is very common in carbon materials including fullerenes,⁷⁰ carbon nanotubes and graphite,⁷¹ graphene⁷² or in boron doped diamond.⁷³

Upon doping the FLG sample with Li and Na, the ESR spectra change significantly: strong signals with about 30-50 times larger intensity appear with an asymmetric lineshape. An asymmetric ESR lineshape is identified as a so-called Dysonian line,¹⁹ which is the usual case in metallic materials. In fact, the Dysonian lineshape in ESR can be considered as analogue to the Fano lineshape in Raman spectroscopy, however its physical origin is different. The Dysonian lineshape is due to the varying microwave phase along the sample volume due to the limited penetration of microwaves. The asymmetry is stronger for both lines in the lithium doped material than in the sodium doped one. This indicates a smaller microwave penetration depth thus a larger conductivity. This observation is in agreement with the visual observations and the Raman spectroscopy results above, *i.e.* that charge transfer is stronger in the lithium doped sample.

Fig. 3. shows that the ESR signal in the alkali doped samples can be decomposed into two distinct ESR lines with different linewidths. The presence of multiple ESR lines is often encountered in alkali atom doped carbon materials. The examples include alkali doped fullerenes^{70,74} and carbon nanotubes (nanotubides).^{54,75} The origin of multiple ESR lines in doped carbon could be an inhomogeneous doping, or the presence of localized paramagnetic spins.

To gain a deeper insight to the electronic properties of the doped materials, the temperature dependence of the ESR signal was studied in the 5

to 250 K temperature range. The ESR intensity is directly proportional to the spin susceptibility, which allows to identify the nature of spins (localized or delocalized) which give rise to the ESR signal. In addition, the ESR linewidth is related to T_2 , which is called the spin-spin relaxation time (due to historical reasons).^{18,19,69} In the following, we refer to this as spin-relaxation time or τ_s to conform with the spintronics literature. Determining τ_s is directly relevant for the spintronics applications of graphene.

The spectroscopic properties, including line intensity, position, and linewidth were determined by fitting the Dysonian lines with a mixture of absorption and dispersion Lorentzian lines,^{76,77} which is a valid approach when the conduction electrons are diffusing through the microwave penetration depth slowly (this is the so-called NMR limit) compared to their lifetime.¹⁹

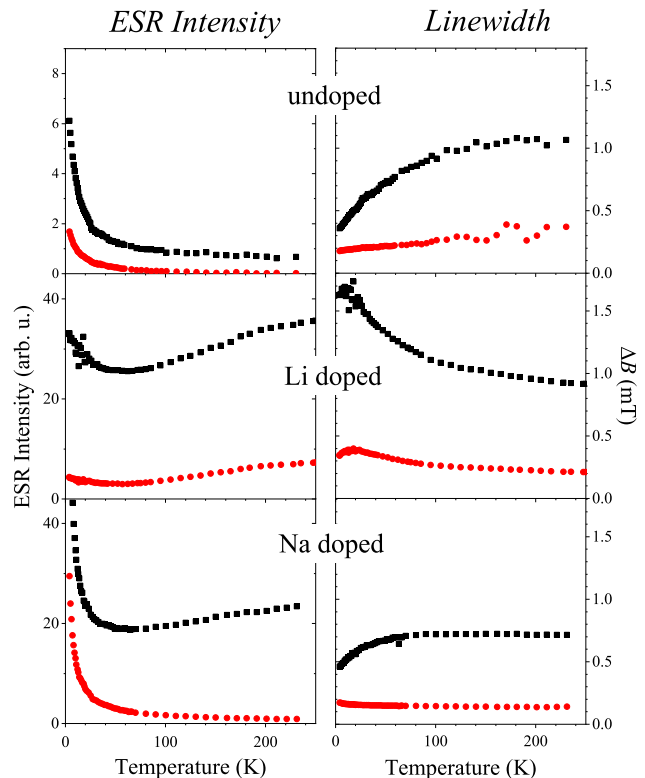


Figure 4: Temperature dependent ESR intensity (normalized by the sample mass) and linewidth. Note the significantly smaller scale for the undoped material. The lithium doped sample shows two Pauli-like signal intensity, which is a clear indication of a metallic behavior. On the other hand, the sodium doped material shows a mixed behavior with one Curie and one Pauli-like signals.

The temperature dependent ESR intensity normalized by the sample mass and the ESR linewidth is shown in Fig. 4. It reinforces the earlier observation that the observed spin susceptibility increases significantly upon doping. In addition, the temperature dependent character of the spin susceptibility also characteristically changes: in the undoped sample, the spin susceptibility shows a significant increase upon lowering temperature, which is characteristic for localized, *i.e.* paramagnetic spin species. We thus term it a "Curie-like" behavior, where $\chi_s \sim 1/T$. In fact, the intensity of the broader peak in the undoped material remains finite at higher temperature. This can be related to an unintentional doping due to some residual solvent or contamination in the starting material.

In contrast, a Pauli-like spin susceptibility, *i.e.* with little temperature dependence, dominates the signal for both the lithium and sodium doped samples above 20 K, although the sodium doped material also contains a Curie-like contribution with a much smaller intensity. An ESR signal with a spin-susceptibility with little or no temperature dependence is characteristic for conduction electrons. The fact, that the Li doped material contains two such signals, hints that the doping is inhomogeneous. We note that the presence of unreacted metallic particles can be excluded as the origin of the observed metallic signals, since metallic Li and Na have a characteristic lineshapes (typical for strongly diffusing electrons) which is not observed herein.^{18,19} Even the Pauli-like signal shows an up-turn in intensity in the Na doped sample below 20 K; similar effects are often encountered when a minute amount (of the 10 ppm level/lattice sites) of paramagnetic spins give a common resonance with the itinerant electrons.⁷⁸ This also means that the linewidth data in the Na doped is only reliable above 20 K.

We identify the Pauli-like signal in the Na doped FLG sample as coming from Na doped graphene monolayers. It is based on the observation that Na cannot dope graphite, thus it is very probable that multilayer graphene is also inaccessible for it. This observation is in a full agreement with the Raman result, as it evidenced that Na doping of an FLG sample leaves a part of the sample undoped.

The ESR linewidth, ΔB , data in Fig. 4 can be used to directly obtain the spin relaxation

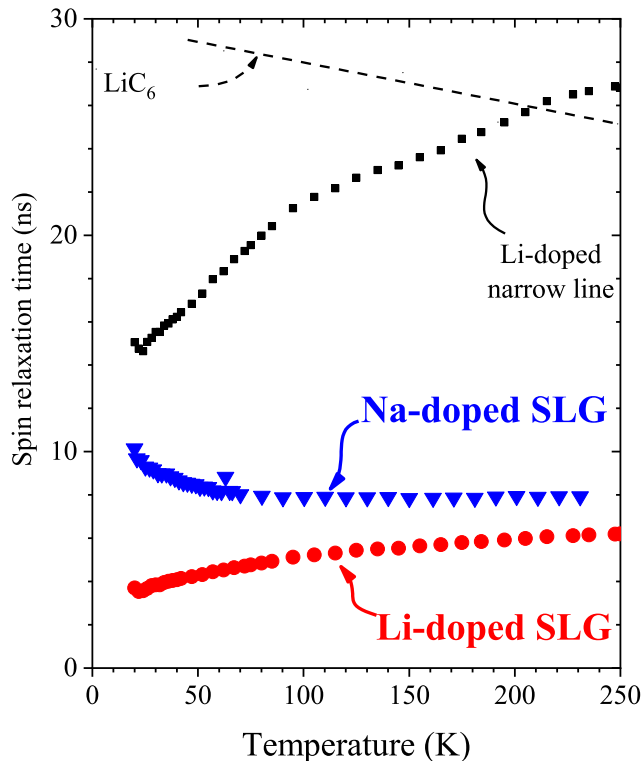


Figure 5: Spin relaxation times of the Li and Na doped few layer graphene above 20 K. Dashed line shows data on the LiC_6 intercalated graphite powder from Ref.⁷⁹

time through $1/\tau_s = 1/\gamma\Delta B$, where $\gamma = 2\pi \cdot 28.0 \text{ GHz/T}$ is the electron gyromagnetic factor. The result is shown in Fig. 5. along with a reference data from LiC_6 intercalated graphite powder from Ref.⁷⁹ The narrow component of the Li doped FLG sample has a relaxation time that is similar to that in LiC_6 . It is therefore tempting to identify this component as coming from Li intercalated graphene multilayers and the broader component to Li doped monolayers. The spin relaxation time of this component is similar to that found for the Na doped graphene monolayers.

In principle, the temperature dependent character of the spin relaxation time also contains information about the relaxation mechanism,^{8,80} whether it can be described by the Elliott-Yafet^{20,21} or the D'yakonov-Perel' theories.⁸¹ However, a proper theoretical description requires the knowledge of the temperature dependent mobility and the local crystalline structure in these samples. Neither of these are available at present, therefore we cannot speculate on the underlying spin-relaxation mechanism.

Nevertheless, the striking observation is that the ESR linewidth at 230 K, when translated to spin-relaxation times, gives ~ 6.1 ns and ~ 7.9 ns for lithium and sodium doped monolayer graphene, respectively. These values are even more surprising in view of the well-known heterogeneity of chemically exfoliated graphene and the synthesis method we employed. In fact, our figures are only surpassed by recent spin-transport experiments on carefully manufactured microscopic graphene samples, with ultrahigh mobility.

Early spin-transport experiments reported sub-nanosecond spin-relaxation times in graphene,^{11,14,15,82–85} which most probably originates from extrinsic effects.⁸⁶ Advanced sample preparation and coating with hexagonal-BN resulted in improved values^{87,88} with the longest spin-relaxation time values being 12.6 ns¹⁶ in single-layer graphene and 9.4 ns in bilayer-graphene.⁸⁹

It is in fact astonishing that a chemically prepared sample, which is readily available in mg quantities, displays the same magnitude for the spin-relaxation time as the above values which are the result of advanced micromanipulation techniques, combined with van der Waals heterostructure engineering. The advanced techniques aim to decrease the defect concentration of individual graphene microstructures. However, bulk, top-down chemical methods may lead to higher quality flakes due to a finite probability that the flake defect concentration may even be smaller than those achieved by local techniques. As the sodium doping can only occur in high-quality single flakes, this may provoke a selectivity that further increases the measured spin-relaxation time, thus leading to the efficient manufacturing of future spintronics materials based on graphene.

CONCLUSIONS

In conclusion, we successfully synthesized lithium and sodium doped few-layer graphene in liquid ammonia solution. We found that Na dopes exclusively monolayer graphene which is present in the FLG sample. This is deduced from an overall weaker Na doping of the FLG samples, which is argued to be associated with the well-

known inability of Na to intercalate graphite, thus multilayer graphene is also inaccessible for it. The obtained materials exhibit a clear change of color, a dominant Fano mode in the Raman spectrum, and ESR signals due to conduction electrons. These observations prove a successful intercalation and charge transfer from the alkali atoms toward graphene. Electron spin resonance spectroscopy indicates a spin-relaxation time of 6-8 ns, which is comparable to the longest values found on ultrahigh mobility graphene flakes using spin-transport methods. Given that we studied a relatively impure and bulk graphene material, these figures are encouraging for the spintronics applications of alkali atom doped graphene.

METHODS

Preparation of the few layer graphene starting material. Few-layer graphene was prepared from saturation potassium doped spherical graphite powder (SGN18, Future Carbon) using DMSO solvent for the wet chemical exfoliation as described previously.^{61,90,91} Chemical exfoliation was finalized using ultrasound tip-sonication, which yields the best quality, as shown in a previous study.⁷² The properties of the starting material are well characterized by atomic force microscopy and Raman spectroscopy, which revealed that restacked few-layer graphene is also present in the sample.⁵⁵ Prior to intercalation, the undoped FLG was heated up to 400 °C for 30 minutes in high vacuum (2×10^{-6} mbar) to remove any residual solvents. It was shown previously Refs.^{55,72} that this does not affect the morphology of the starting FLG.

Doping of graphene with lithium and sodium Lithium and sodium with a purity of 99.9 + % and 99.8% (from Sigma-Aldrich), respectively, were handled in an Ar glove box ($O_2, H_2O < 0.1$ ppm). The lithium granules had metallic color and were cut into smaller pieces to increase the surface. The sodium chunks were first thoroughly cleaned and then cut up. About 1 milligram of FLG and excess alkali metal of 1.1 or 2.2 milligrams for lithium and sodium, respectively, were placed in a bulb shaped quartz container (reaction chamber in the following) inside the glove box. The bulb of the re-

action chamber (hand-blown by a technician) had a diameter of 10 mm and it was connected to the vacuum line with a 5 mm diameter quartz tube. A (Li,Na)C₆ stoichiometry (which is probably the upper limit of doping) would require 0.09 mg and 0.24 mg for the Li and Na, respectively, for the 1 mg FLG. The unreacted mixture was then connected to a vacuum line with the help of a well-sealing valve and pumped to a vacuum better than 10⁻⁶ mbar.

The reaction chamber was placed in liquid nitrogen and gaseous ammonia, that was connected to the vacuum line, was rapidly (within a few seconds) condensed to the starting mixture of FLG and alkali metal. The rapid condensing is required to prevent the formation of side products. Following this, the reaction chamber is surrounded by an ethanol bath which is kept at -40 °C (below the -33 °C boiling point of ammonia at ambient pressure). Ethanol has a freezing point of -114 °C thus it is well suited for this purpose. The reaction chamber, surrounded by the ethanol bath was immersed in a bath sonicator where it was intensively sonicated for 30 minutes to obtain a homogeneous doping of the few-layer graphene. The pressure of the chamber is monitored to avoid evaporation of the ammonia during the process. The dissolution of alkali metals in liquid ammonia can be followed by characteristic color changes: the solution changes its color to dark blue initially, immediately followed by a change to yellow-brownish. This marks the dissolution of the alkali metals: dark blue color indicates a low concentration of the dissolved alkali and yellow-brownish color is characteristic for a high concentration of dissolved alkali metals.⁹² Finally, the reaction chamber changes its color to a homogeneous brown which indicates the doping of FLG with the alkali metals.

At the end of the intercalation, the solution is slowly heated to room temperature, when ammonia is evacuated. Subsequently, a heating of 200 °C is applied for 30 minutes to remove any absorbed ammonia and the unreacted alkali metal. The choice of 200 °C is delicate: on one hand it is above the melting temperature of the alkali metals (181 °C for Li and 98 °C for Na) which allows for an efficient removal of the unreacted, excess alkali atoms but on the other hand, it is below the

onset of the formation temperature of alkali carbides (this occurs above ~ 400 °C, Ref.⁹³). The reaction chambers were sealed off with a torch on the 5 mm quartz tube part.

Ammonia is known to react with alkali metal elements and forms amides.^{94,95} This side reaction is known to proceed fast when the ammonia is in the gas phase. However, this reaction channel is prohibited (or slowed down to the week timescale), when the ammonia is liquefied. Besides, the amides have well-known signatures in Raman spectroscopy^{96,97} in the form of a series of lines around 400 – 550 cm⁻¹. These signals were used to monitor the content of this unwanted side product. We optimized the procedure to yield a material with no traces of amides.⁹⁸ We emphasize at this point that while we refer to the material as "Na doped FLG", Na dopes exclusively the monolayer graphene content inside the sample.

Raman spectroscopy. Raman spectroscopy was performed on the as prepared samples inside the same reaction chambers where the doping proceeds. A 514.5 nm wavelength laser excitation with 0.5 mW power was used to avoid laser-induced deintercalation^{56,99} or sample heating. Raman spectra were recorded on a modified broadband LabRAM spectrometer (Horiba Jobin-Yvon Inc.). The built-in interference filter was replaced by a beam splitter plate with 30% reflection and 70% transmission to allow for a broadband operation.^{100,101} Typically 0.5 mW laser powers were used with a built-in microscope (Olympus LMPlan 50 × /0.50 inf./0/NN26.5), which yields about 1 μm × 1 μm spot size. Photographs were taken with an Olympus 10 × / 50× objective, which is present on the LabRAM equipment.

Electron spin resonance The reaction chambers were opened up inside an Ar glove box and placed into quartz tubes with a 4 mm outer diameter. These tubes were then evacuated on the vacuum line to better than 2 × 10⁻⁶ mbar, then filled with 20 mbar He exchange gas for the cryogenic measurements and sealed permanently with a torch. Raman spectrum of the materials were checked before and after this procedure to ensure that no changes occur during this operation. ESR measurements were performed on a Bruker Elexsys E500 X-band spectrometer equipped with an Oxford He flow cryostat. The temperature

could be varied between 4 and 300 K. Care was taken to avoid saturation and overmodulation of the observed signals, similarly to our previous works.^{54,102} The spectral parameters of each signal component is determined by fitting (derivative) Lorentzian and Dysonian curves, as is customary in the ESR literature. Due to the magnetic field modulation technique employed in ESR, the observed lineshapes are the derivative of the following (with respect to the magnetic field, B):

$$I(B) = A \cdot \frac{\Delta B \cos(\phi) + (B - B_0) \sin(\phi)}{(B - B_0)^2 + \Delta B^2}, \quad (2)$$

where the ESR lineshape, $I(B)$ is given as a function of the B magnetic field, A is proportional to the static spin susceptibility, B_0 is the line position, ΔB is the ESR linewidth, ϕ is the mixing angle between the two types of curves (absorption and dispersion). The ESR linewidth is related to the T_2 spin-spin relaxation time as $\Delta B = 1/\gamma T_2$ where $\gamma = 2\pi \cdot 28.0 \text{ GHz/T}$ is the so-called electron gyromagnetic ratio.

Magnetometry with a superconducting quantum interference device Samples inside the same, He exchange gas filled quartz tubes were used for the SQUID measurement that were used in the ESR studies. We searched for traces of superconductivity in a standard MPMS SQUID magnetometer down to 2 K with a zero magnetic field cooling protocol, in small applied fields of 5 – 50 Oe, and also at 2 K in magnetic hysteresis loops.

ASSOCIATED CONTENT

Supporting Information

The Supporting Information is available free of charge at <https://pubs.acs.org/doi/.....>

Details of the Raman spectra deconvolution, spectroscopic parameters of the Breit-Wigner-Fano lineshapes, a discussion of the electron-phonon coupling and the temperature dependent g -factor as detected by electron spin resonance (PDF).

AUTHOR INFORMATION

Author Contributions

B.G.M. performed the doping, Raman and ESR studies under the supervision of F.S., P.Sz., B.N. and L.F. contributed to the Raman and ESR investigations. K. E., P. E. prepared the starting FLG samples under the supervision of A. H and F. H. SQUID measurement were performed by N. M. N. Raman studies and the analysis was performed by J.C.C-T. and T. P. All authors contributed to the writing of the manuscript.

Notes

The authors declare no competing financial interest.

ACKNOWLEDGEMENTS

The Authors are indebted to András Magyar for the preparation of the reaction chambers. We wish to kindly thank Prof. J. L. Martinez for performing the SQUID measurements. Support by the National Research, Development and Innovation Office of Hungary (NKFIH) Grant Nrs. K119442 and 2017-1.2.1-NKP-2017-00001 are acknowledged. T. P. thanks the FWF (P27769-N20) for funding.

SUPPLEMENTARY MATERIAL

Deconvolution of the Raman spectra

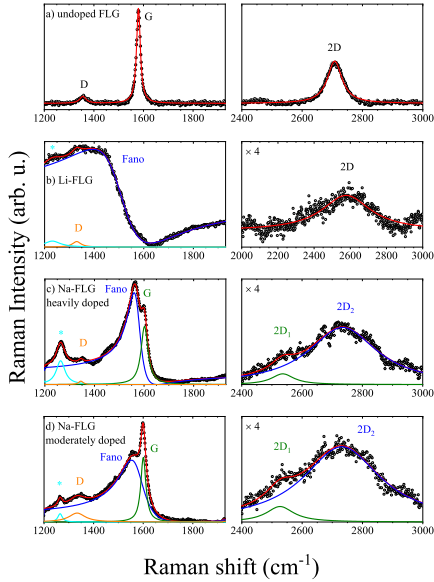


Figure S1: Deconvolution of the observed Raman spectra for the various samples.

Deconvolution of the observed Raman spectra is depicted in Fig. S1. The sum of the lines are shown in red. On the left side, the asymmetric Fano lineshape is denoted with blue color. The peak only present around 1600 cm^{-1} in the sodium species are green. The D mode has an orange color in the figure. The parasitic signal arising from the quartz tube is marked with * and shown in cyan color. On the right side, the extremely broadened 2D mode is shown. For the case of lithium it composes only a single Lorentzian, while for sodium it splits into two. This is probably related to the argument that only the monolayer flakes get truly charged.

We note that in LiC_6 (Ref.⁵⁶), the transformation of the G mode to a dominant Fano lineshape is accompanied by the complete disappearance of the 2D mode, which is not the case herein. This is probably related to the sample heterogeneity and the resulting inhomogeneous doping in agreement

with Fig. 1b. of the main text, where the characteristic red/golden spots of a highly intercalated Li compound are not homogeneously dispersed along the sample. Also, we cannot exclude that besides the dominant Fano line, a small G mode (corresponding to un- or weakly doped graphene layers) exists, whose presence is suggested from the strongly broadened 2D-mode observed in Fig. S1b., which in single LiC_6 crystals is not present.⁵⁶

The obtained parameters from the fit of the G mode related peaks are summarized in Table 1. The complete deconvolution of the observed peaks are visualized in Fig. S1. The electron-phonon coupling parameter is calculated from the fitted values, as described later.

To obtain further valuable information of the nature lithium intercalation, the electron-phonon coupling parameter (EPC), which is directly related to the charge transfer can be calculated from the the fitted parameters, whose are summarized in Table 1 and Figure S1 of Supplementary Materials, using:

$$\gamma^{\text{EPC}} = 2\sqrt{(\omega_{\text{Fano}} - \omega_{\text{A}})(\omega_{\text{NA}} - \omega_{\text{Fano}})}. \quad (3)$$

Here, ω_{Fano} is the measured position of the G-line peak, ω_{A} and ω_{NA} are the calculated adiabatic and non-adiabatic phonon frequencies.¹⁰³ We approximate the latter two quantities with the ones calculated for LiC_6 : $\omega_{\text{A}} = 1362 \text{ cm}^{-1}$ and $\omega_{\text{NA}} = 1580 \text{ cm}^{-1}$, as no exact calculation exists for FLG. This approximation was found to be valid in similar hexagonal carbon systems such as potassium doped multiwalled carbon nanotubes.¹⁰⁴ The calculated EPC value for the lithium doped sample is $\gamma^{\text{EPC}} = 206 \text{ cm}^{-1}$, which is similar to that of LiC_6 , where it is 157 cm^{-1} .⁵⁶ Unfortunately, no adequate calculation exists for the case of sodium.

Change of g -factor upon alkali intercalation

ESR g -factors of the investigated materials are shown in Fig. S2. with respect to that of $g_{\text{undoped,narrowline,50 K}} = 2.0069$ of the narrow line of the undoped material at 50 K. Please note that each line present in the intercalated materials are

Table 1: Obtained parameters of the fitted Raman modes. The position and width values are in cm^{-1} .

Sample	ω_G	Γ_G	ω_{Fano}	Γ_{Fano}	q	γ^{EPC}
Undoped	1580	10				
Li-doped			1507	116	-1.03	206
LiC ₆ [Ref. ⁵⁶]	1585	71	1546	71	-1.09	157
Na-doped (heavily)	1602	16	1572	31	-2.64	
Na-doped (moderately)	1600	16	1572	61	-3.17	

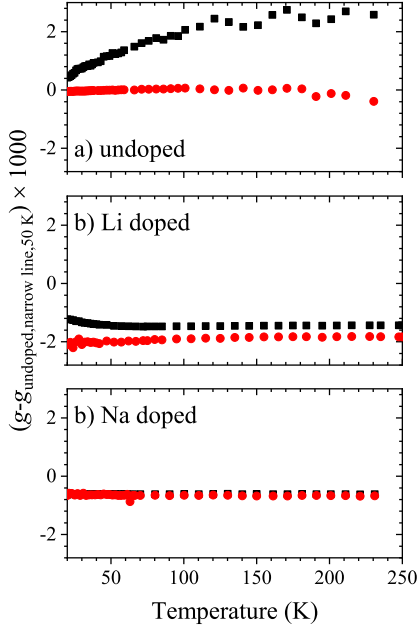


Figure S2: Relative g -factor values compared to $g_{\text{undoped,narrow line,50 K}} = 2.0069$, which corresponds the narrow line of the undoped material at 50 K. Please note, that both lines in the intercalated materials are downshifted, which is expected according to the Elliott-Yafet theory.^{20,21}

downshifted relative to this, which is an expected behavior upon n doping, according to the Elliott-Yafet theory.^{20,21} This is also a clear indication of charge transfer and successful intercalation.

REFERENCES

- (1) Korthauer, R. *Lithium-Ion Batteries: Basics and Applications*; Springer-Verlag GmbH: Berlin, Germany, 2018.
- (2) Emery, N.; Hérold, C.; d’Astuto, M.; Garcia, V.; Bellin, C.; Marêché, J. F.; Lagrange, P.; Loupiau, G. Superconductivity of Bulk CaC₆. *Phys. Rev. Lett.* **2005**, *95*, 087003.
- (3) Emery, N.; Hérold, C.; Marêché, J.-F.; Lagrange, P. Synthesis and Superconducting Properties of CaC₆. *Sci. Technol. Adv. Mater.* **2008**, *9*, 044102.
- (4) Rosseinsky, M. J.; Ramirez, A. P.; Glarum, S. H.; Murphy, D. W.; Haddon, R. C.; Hebard, A. F.; Palstra, T. T. M.; Kortan, A. R.; Zahurak, S. M.; Makhija, A. V. Superconductivity at 28 K in Rb_xC₆₀. *Phys. Rev. Lett.* **1991**, *66*, 2830–2832.
- (5) Jánossy, A.; Nemes, N.; Fehér, T.; Oszlányi, G.; Baumgartner, G.; Forró, L. Antiferromagnetic Resonance in the Linear Chain Conducting Polymers RbC₆₀ and CsC₆₀. *Phys. Rev. Lett.* **1997**, *79*, 2718–2721.
- (6) Ishii, H.; Kataura, H.; Shiozawa, H.; Yoshioka, H.; Otsubo, H.; Takayama, Y.; Miyahara, T.; Suzuki, S.; Achiba, Y.; Nakatake, M.; Narimura, T.; Higashiguchi, M.; Shimada, K.; Taniguchi, M. Direct Observation of Tomonaga-Luttinger-Liquid State in Carbon Nanotubes at Low Temperatures. *Nature* **2003**, *426*, 540–544.
- (7) Rauf, H.; Pichler, T.; Knupfer, M.; Fink, J.; Kataura, H. Transition from a Tomonaga-Luttinger Liquid to a Fermi Liquid in

- Potassium-Intercalated Bundles of Single-Wall Carbon Nanotubes. *Phys. Rev. Lett.* **2004**, *93*, 096805.
- (8) Žutić, I.; Fabian, J.; Das Sarma, S. Spintronics: Fundamentals and Applications. *Rev. Mod. Phys.* **2004**, *76*, 323–410.
- (9) Wolf, S. A.; Awschalom, D. D.; Buhrman, R. A.; Daughton, J. M.; von Molnár, S.; Roukes, M. L.; Chtchelkanova, A. Y.; Treger, D. M. Spintronics: A Spin-Based Electronics Vision for the Future. *Science* **2001**, *294*, 1488–1495.
- (10) Wu, M. W.; Jiang, J. H.; Weng, M. Q. Spin Dynamics in Semiconductors. *Phys. Rep.* **2010**, *493*, 61–236.
- (11) Tombros, N.; Józsa, C.; Popinciuc, M.; Jonkman, H. T.; van Wees, B. J. Electronic Spin Transport and Spin Precession in Single Graphene Layers at Room Temperature. *Nature* **2007**, *448*, 571–574.
- (12) Han, W.; Kawakami, R. K. Spin Relaxation in Single-Layer and Bilayer Graphene. *Phys. Rev. Lett.* **2011**, *107*, 047207.
- (13) Yang, T.-Y.; Balakrishnan, J.; Volmer, F.; Avsar, A.; Jaiswal, M.; Samm, J.; Ali, S. R.; Pachoud, A.; Zeng, M.; Popinciuc, M.; Güntherodt, G.; Beschoten, B.; Özyilmaz, B. Observation of Long Spin-Relaxation Times in Bilayer Graphene at Room Temperature. *Phys. Rev. Lett.* **2011**, *107*, 047206.
- (14) Avsar, A.; Yang, T.-Y.; Bae, S.; Balakrishnan, J.; Volmer, F.; Jaiswal, M.; Yi, Z.; Ali, S. R.; Güntherodt, G.; Hong, B. H.; Beschoten, B.; Özyilmaz, B. Toward Wafer Scale Fabrication of Graphene Based Spin Valve Devices. *Nano Lett.* **2011**, *11*, 2363–2368.
- (15) Han, W.; Chen, J.-R.; Wang, D.; McCreary, K. M.; Wen, H.; Swartz, A. G.; Shi, J.; Kawakami, R. K. Spin Relaxation in Single-Layer Graphene with Tunable Mobility. *Nano Lett.* **2012**, *12*, 3443–3447.
- (16) Drögeler, M.; Franzen, C.; Volmer, F.; Pohlmann, T.; Banszerus, L.; Wolter, M.; Watanabe, K.; Taniguchi, T.; Stampfer, C.; Beschoten, B. Spin Lifetimes Exceeding 12 ns in Graphene Nonlocal Spin Valve Devices. *Nano Lett.* **2016**, *16*, 3533–3539.
- (17) Kochan, D.; Gmitra, M.; Fabian, J. Spin Relaxation Mechanism in Graphene: Resonant Scattering by Magnetic Impurities. *Phys. Rev. Lett.* **2014**, *112*, 116602.
- (18) Feher, G.; Kip, A. F. Electron Spin Resonance Absorption in Metals. I. Experimental. *Phys. Rev.* **1955**, *95*, 337–348.
- (19) Dyson, F. J. Electron Spin Resonance Absorption in Metals. II. Theory of Electron Diffusion and the Skin Effect. *Phys. Rev.* **1955**, *98*, 349–359.
- (20) Elliott, R. J. Theory of the Effect of Spin-Orbit Coupling on Magnetic Resonance in Some Semiconductors. *Phys. Rev.* **1954**, *96*, 266–279.
- (21) Yafet, Y. g -Factors and Spin-Lattice Relaxation of Conduction Electrons. *Solid State Phys.* **1963**, *14*, 1–98.
- (22) Dresselhaus, M. S.; Dresselhaus, G. Intercalation Compounds of Graphite. *Adv. Phys.* **1981**, *30*, 139–326.
- (23) Jung, N.; Kim, B.; Crowther, A. C.; Kim, N.; Nuckolls, C.; Brus, L. Optical Reflectivity and Raman Scattering in Few-Layer-Thick Graphene Highly Doped by K and Rb. *ACS Nano* **2011**, *5*, 5708–5716.
- (24) Howard, C. A.; Dean, M. P. M.; Withers, F. Phonons in Potassium-Doped Graphene: The Effects of Electron-phonon Interactions, Dimensionality, and Adatom Ordering. *Phys. Rev. B* **2011**, *84*, 241404(R).
- (25) Kumar, A.; Reddy, A. L. M.; Mukherjee, A.; Dubey, M.; Zhan, X.; Singh, N.; Ci, L.; Billups, W. E.; Nagurny, J.; Mital, G.; Ajayan, P. M. Direct Synthesis of Lithium-Intercalated Graphene for Electrochemical Energy Storage Application. *ACS Nano* **2011**, *5*, 4345–4349.

- (26) Xue, M.; Chen, G.; Yang, H.; Zhu, Y.; Wang, D.; He, J.; Cao, T. Superconductivity in Potassium-Doped Few-Layer Graphene. *J. Am. Chem. Soc.* **2012**, *134*, 6536–6539.
- (27) Parret, R.; Paillet, M.; Huntzinger, J.-R.; Nakabayashi, D.; Michel, T.; Tiberj, A.; Sauvajol, J.-L.; Zahab, A. A. *In Situ* Raman Probing of Graphene over a Broad Doping Range upon Rubidium Vapor Exposure. *ACS Nano* **2013**, *7*, 165–173.
- (28) Zhou, E.; Xi, J.; Liu, Y.; Xu, Z.; Guo, Y.; Peng, L.; Gao, W.; Ying, J.; Chen, Z.; Gao, C. Large-Area Potassium-Doped Highly Conductive Graphene Films for Electromagnetic Interference Shielding. *Nanoscale* **2017**, *9*, 18613–18618.
- (29) Pervan, P.; Lazić, P. Adsorbed or Intercalated: Na on Graphene/Ir(111). *Phys. Rev. Mater.* **2017**, *1*, 044202.
- (30) Wang, G.; Shen, X.; Yao, J.; Park, J. Graphene Nanosheets for Enhanced Lithium Storage in Lithium Ion Batteries. *Carbon* **2013**, *47*, 2049–2053.
- (31) Yang, X.; Cheng, C.; Wang, Y.; Qiu, L.; Li, D. Liquid-Mediated Dense Integration of Graphene Materials for Compact Capacitive Energy Storage. *Science* **2013**, *341*, 534–537.
- (32) Mahmood, N.; Zhang, C.; Yin, H.; Hou, Y. Graphene-Based Nanocomposites for Energy Storage and Conversion in Lithium Batteries, Supercapacitors and Fuel Cells. *J. Mater. Chem. A* **2014**, *2*, 15–32.
- (33) Medarde, M.; Mena, M.; Gavilano, J. L.; Pomjakushina, E.; Sugiyama, J.; Kamazawa, K.; Pomjakushin, V. Y.; Sheptyakov, D.; Batlogg, B.; Ott, H. R.; Månsson, M.; Juranyi, F. 1D to 2D Na⁺ Ion Diffusion Inherently Linked to Structural Transitions in Na_{0.7}CoO₂. *Phys. Rev. Lett.* **2013**, *110*, 266401.
- (34) Barpanda, P.; Oyama, G.; Ichi Nishimura, S.; Chung, S.-C.; Yamada, A. A 3.8-V Earth-Abundant Sodium Battery Electrode. *Nat. Commun.* **2014**, *5*, 4358.
- (35) Ares, P.; Palacios, J. J.; Abellán, G.; Gómez-Herrero, J.; Zamora, F. Recent Progress on Antimonene: A New Bidimensional Material. *Adv. Mater.* **2017**, *30*, 1703771.
- (36) Tian, W.; Zhang, S.; Huo, C.; Zhu, D.; Li, Q.; Wang, L.; Ren, X.; Xie, L.; Guo, S.; Chu, P. K.; Zeng, H.; Huo, K. Few-Layer Antimonene: Anisotropic Expansion and Reversible Crystalline-Phase Evolution Enable Large-Capacity and Long-Life Na-Ion Batteries. *ACS Nano* **2018**, *12*, 1887–1893.
- (37) Asher, R. C.; Wilson, S. A. Lamellar Compound of Sodium with Graphite. *Nature* **1958**, *181*, 409–410.
- (38) Asher, R. C. A Lamellar Compound of Sodium and Graphite. *J. Inorg. Nucl. Chem.* **1959**, *10*, 238–249.
- (39) Metrot, A.; Guerard, D.; Billaud, D.; Herold, A. New Results About the Sodium-Graphite System. *Synth. Met.* **1980**, *1*, 363–369.
- (40) Akuzawa, N.; Yoshioka, J.; Ozaki, C.; Tokuda, M.; Ohkura, K.; Soneda, Y. Preparation and Characterization of Sodium-Graphite Intercalation Compounds. *Mol. Cryst. Liq. Cryst.* **2002**, *388*, 1–7.
- (41) Lenchuk, O.; Adelhelm, P.; Mollenhauer, D. New Insights into the Origin of Unstable Sodium Graphite Intercalation Compounds. *Phys. Chem. Chem. Phys.* **2019**, *21*, 19378–19390.
- (42) Choucair, M.; Thordarson, P.; Stride, J. A. Gram-Scale Production of Graphene Based on Solvothermal Synthesis and Sonication. *Nat. Nanotechnol.* **2009**, *4*, 30.
- (43) Pramudita, J.; Rawal, A.; Choucair, M.; Pontiroli, D.; Magnani, G.; Gaboardi, M.; Ricco, M.; Sharma, N. Mechanisms of Sodium Insertion/Extraction on the Surface of Defective Graphenes. *ACS Appl. Mater. Interfaces* **2016**, *9*.

- (44) Quan, B.; Jin, A.; Yu, S.-H.; Kang, S. M.; Jeong, J.; Abruña, H. D.; Jin, L.; Piao, Y.; Sung, Y.-E. Solvothermal-Derived S-Doped Graphene as an Anode Material for Sodium-Ion Batteries. *Adv. Sci.* **2018**, *5*, 1700880.
- (45) Beguin, F.; Setton, R.; Beguin, F.; Setton, R.; Hamwi, A.; Touzain, P. The Reversible Intercalation of Tetrahydrofuran in Some Graphite-Alkali Metal Lamellar Compounds. *Mater. Sci. Eng.* **1979**, *40*, 167–173.
- (46) Mizutani, Y.; Ihara, E.; Abe, T.; Asano, M.; Harada, T.; Ogumi, Z.; Inaba, M. Preparation of Alkali Metal Graphite Intercalation Compounds in Organic Solvents. *J. Phys. Chem. Solids* **1996**, *57*, 799–803.
- (47) Mizutani, Y.; Abe, T.; Inaba, M.; Ogumi, Z. Creation of Nanospaces by Intercalation of Alkali Metals Into Graphite in Organic Solutions. *Synth. Met.* **2001**, *125*, 153–159.
- (48) Murphy, D. W.; Rosseinsky, M. J.; Fleming, R. M.; Tycko, R.; Ramirez, A. P.; Haddon, R. C.; Siegrist, T.; Dabbagh, G.; Tully, J. C.; Walstedt, R. E. Synthesis and Characterization of Alkali Metal Fullerides: A_xC_{60} . *J. Phys. Chem. Solids* **1992**, *53*, 1321–1332.
- (49) Buffinger, D. R.; Ziebarth, R. P.; Stenger, V. A.; Recchia, C.; Pennington, C. H. Rapid and Efficient Synthesis of Alkali Metal- C_{60} Compounds in Liquid Ammonia. *J. Am. Chem. Soc.* **1993**, *115*, 9267–9270.
- (50) Dahlke, P.; Denning, M. S.; Henry, P. F.; Rosseinsky, M. J. Superconductivity in Expanded FCC C_{60}^{3-} Fullerides. *J. Am. Chem. Soc.* **2000**, *122*, 12352–12361.
- (51) Kumar, A.; Reddy, A. L. M.; Mukherjee, A.; Dubey, M.; Zhan, X.; Singh, N.; Ci, L.; Billups, W. E.; Nagurny, J.; Mital, G.; Ajayan, P. M. Direct Synthesis of Lithium-Intercalated Graphene for Electrochemical Energy Storage Application. *ACS Nano* **2011**, *5*, 4345–4349.
- (52) Ganin, A. Y.; Takabayashi, Y.; Jeglič, P.; Arčon, D.; Potočnik, A.; Baker, P. J.; Ohishi, Y.; McDonald, M. T.; Tzirakis, M. D.; McLennan, A.; Darling, G. R.; Takata, M.; Rosseinsky, M. J.; Prassides, K. Polymorphism Control of Superconductivity and Magnetism in Cs_3C_{60} Close to the Mott Transition. *Nature* **2010**, *466*, 221–225.
- (53) Hirsch, A. *The Chemistry of the Fullerenes*; WILEY-VCH Verlag GmbH & Co. KGaA: Weinheim, Germany, 2002.
- (54) Szirmai, P.; Márkus, B. G.; Dóra, B.; Fábrián, G.; Koltai, J.; Zólyomi, V.; Kürti, J.; Náfrádi, B.; Forró, L.; Pichler, T.; Simon, F. Doped Carbon Nanotubes as a Model System of Biased Graphene. *Phys. Rev. B* **2017**, *96*, 075133.
- (55) Szirmai, P.; Márkus, B. G.; Chacón-Torres, J. C.; Eckerlein, P.; Edelthammer, K.; Englert, J. M.; Mundloch, U.; Hirsch, A.; Hauke, F.; Náfrádi, B.; Forró, L.; Kramberger, C.; Pichler, T.; Simon, F. Characterizing the Maximum Number of Layers in Chemically Exfoliated Graphene. *Sci. Rep.* **2019**, *9*, 19480.
- (56) Chacón-Torres, J. C.; Ganin, A. Y.; Rosseinsky, M. J.; Pichler, T. Raman Response of Stage-1 Graphite Intercalation Compounds Revisited. *Phys. Rev. B* **2012**, *86*, 075406.
- (57) Udod, I. A.; Genchel, V. K. Synthesis Under High Pressure and X-rays Study Graphite Intercalation Compounds of Sodium. *High Pressure Res.* **1992**, *8*, 581–586.
- (58) Oszlányi, G.; Baumgartner, G.; Faigel, G.; Forró, L. Na_4C_{60} : An Alkali Intercalated Two-Dimensional Polymer. *Phys. Rev. Lett.* **1997**, *78*, 4438–4441.
- (59) Brouet, V.; Alloul, H.; Le, T.-N.; Garaj, S.; Forró, L. Role of Dynamic Jahn-Teller Distortions in Na_2C_{60} and Na_2CsC_{60} Studied by NMR. *Phys. Rev. Lett.* **2001**, *86*, 4680–4683.

- (60) Brouet, V.; Alloul, H.; Garaj, S.; Forró, L. Gaps and Excitations in Fullerides with Partially Filled Bands: NMR Study of Na_2C_{60} and K_4C_{60} . *Phys. Rev. B* **2002**, *66*, 155122.
- (61) Englert, J. M.; Dotzer, C.; Yang, G.; Schmid, M.; Papp, C.; Gottfried, J. M.; Steinrück, H.-P.; Spiecker, E.; Hauke, F.; Hirsch, A. Covalent Bulk Functionalization of Graphene. *Nat. Chem.* **2011**, *3*, 279–286.
- (62) Fano, U. Effects of Configuration Interaction on Intensities and Phase Shifts. *Phys. Rev.* **1961**, *124*, 1866–1878.
- (63) Kuzmany, H. *Solid-State Spectroscopy, An Introduction*, 2nd ed.; Springer-Verlag: Vienna, Austria, 2009.
- (64) Chacón-Torres, J. C.; Wirtz, L.; Pichler, T. Manifestation of Charged and Strained Graphene Layers in the Raman Response of Graphite Intercalation Compounds. *ACS Nano* **2013**, *7*, 9249–9259.
- (65) Kuzmany, H.; Matus, M.; Burger, B.; Winter, J. Raman Scattering in C_{60} Fullerenes and Fullerides. *Adv. Mater.* **1994**, *6*, 731–745.
- (66) Rao, A. M.; Eklund, P. C.; Bandow, S.; Thess, A.; Smalley, R. E. Evidence for Charge Transfer in Doped Carbon Nanotube Bundles from Raman Scattering. *Nature* **1997**, *388*, 257–259.
- (67) Eklund, P. C.; Dresselhaus, G.; Dresselhaus, M. S.; Fischer, J. E. Raman Scattering from Inplane Lattice Modes in Low-Stage Graphite-Alkali-Metal Compounds. *Phys. Rev. B* **1977**, *16*, 3330–3333.
- (68) Weller, T. E.; Ellerby, M.; Saxena, S. S.; Smith, R. P.; Skipper, N. T. Superconductivity in the Intercalated Graphite Compounds C_6Yb and C_6Ca . *Nature Physics* **2005**, *1*, 39–41.
- (69) Slichter, C. P. *Principles of Magnetic Resonance*, 2nd ed.; Springer: New York, USA, 1989.
- (70) Nemes, N. M.; Fischer, J. E.; Baumgartner, G.; Forró, L.; Fehér, T.; Oszlányi, G.; Simon, F.; Jánossy, A. Conduction-electron Spin Resonance in the Superconductor K_3C_{60} . *Phys. Rev. B* **2000**, *61*, 7118–7121.
- (71) Galambos, M. et al. Identifying the Electron Spin Resonance of Conduction Electrons in Alkali Doped SWCNTs. *Phys. Status Solidi B* **2009**, *246*, 2760–2763.
- (72) Márkus, B. G.; Simon, F.; Chacón-Torres, J. C.; Reich, S.; Szirmai, P.; Náfrádi, B.; Forró, L.; Pichler, T.; Vecera, P.; Hauke, F.; Hirsch, A. Transport, Magnetic and Vibrational Properties of Chemically Exfoliated Few-Layer Graphene. *Phys. Status Solidi B* **2015**, *252*, 2438–2443.
- (73) Szirmai, P.; Fábián, G.; Koltai, J.; Náfrádi, B.; Forró, L.; Pichler, T.; Williams, O. A.; Mandal, S.; Bäuerle, C.; Simon, F. Observation of Conduction Electron Spin Resonance in Boron-Doped Diamond. *Phys. Rev. B* **2013**, *87*, 195132.
- (74) Jánossy, A.; Chauvet, O.; Pekker, S.; Cooper, J. R.; Forró, L. Conduction Electron Spin Resonance in Rb_3C_{60} . *Phys. Rev. Lett.* **1993**, *71*, 1091–1094.
- (75) Claye, A. S.; Nemes, N. M.; Jánossy, A.; Fischer, J. E. Structure and Electronic Properties of Potassium-Doped Single-Wall Carbon Nanotubes. *Phys. Rev. B* **2000**, *62*, R4845–R4848.
- (76) Walmsley, L. Translating Conduction-Electron Spin-Resonance Lines into Lorentzian Lines. *J. Magn. Reson., Ser. A* **1996**, *122*, 209–213.
- (77) Djokić, D. M.; Stepanenko, D.; Dohčević-Mitrović, Z. Extreme Conduction Electron Spin Resonance: $A/B \rightarrow (5 + 3\sqrt{3})/4$, the Universal Limit of Lineshape Asymmetry Ratio. *J. Magn. Magn. Mater.* **2019**, *491*, 165616.

- (78) Barnes, S. E. Theory of Electron Spin Resonance of Magnetic Ions in Metals. *Adv. Phys.* **1981**, *30*, 801–938.
- (79) Lauginie, P.; Estrade, H.; Conard, J.; Guérard, D.; Lagrange, P.; El Makrini, M. Graphite Lamellar Compounds ESR Studies. *Physica B* **1980**, *99*, 514–520.
- (80) Tsymbal, E. Y.; Žutić, I. *Handbook of Spin Transport and Magnetism*; Taylor & Francis: New York, USA, 2012.
- (81) Dyakonov, M. I.; Perel, V. I. Spin Relaxation of Conduction Electrons in Noncentrosymmetric Semiconductors. *Sov. Phys. Solid State Phys.* **1971**, *13*, 3023.
- (82) Han, W.; Pi, K.; McCreary, K. M.; Li, Y.; Wong, J. J. I.; Swartz, A. G.; Kawakami, R. K. Tunneling Spin Injection into Single Layer Graphene. *Phys. Rev. Lett.* **2010**, *105*, 167202.
- (83) Yang, T.-Y.; Balakrishnan, J.; Volmer, F.; Avsar, A.; Jaiswal, M.; Samm, J.; Ali, S. R.; Pachoud, A.; Zeng, M.; Popinciuc, M.; Güntherodt, G.; Beschoten, B.; Özyilmaz, B. Observation of Long Spin-Relaxation Times in Bilayer Graphene at Room Temperature. *Phys. Rev. Lett.* **2011**, *107*, 047206.
- (84) Han, W.; Kawakami, R. K. Spin Relaxation in Single-Layer and Bilayer Graphene. *Phys. Rev. Lett.* **2011**, *107*, 047207.
- (85) Volmer, F.; Drögeler, M.; Maynicke, E.; von den Driesch, N.; Boschen, M. L.; Güntherodt, G.; Beschoten, B. Role of MgO Barriers for Spin and Charge Transport in Co/MgO/Graphene Nonlocal Spin-Valve Devices. *Phys. Rev. B* **2013**, *88*, 161405.
- (86) Kochan, D.; Gmitra, M.; Fabian, J. Spin Relaxation Mechanism in Graphene: Resonant Scattering by Magnetic Impurities. *Phys. Rev. Lett.* **2014**, *112*, 116602.
- (87) Drögeler, M.; Volmer, F.; Wolter, M.; Terrés, B.; Watanabe, K.; Taniguchi, T.; Güntherodt, G.; Stampfer, C.; Beschoten, B. Nanosecond Spin Lifetimes in Single- and Few-Layer Graphene–hBN Heterostructures at Room Temperature. *Nano Lett.* **2014**, *14*, 6050–6055.
- (88) Guimarães, M. H. D.; Zomer, P. J.; Inglá-Aynés, J.; Brant, J. C.; Tombros, N.; van Wees, B. J. Controlling Spin Relaxation in Hexagonal BN-Encapsulated Graphene with a Transverse Electric Field. *Phys. Rev. Lett.* **2014**, *113*, 086602.
- (89) Leutenantsmeyer, J. C.; Inglá-Aynés, J.; Fabian, J.; van Wees, B. J. Observation of Spin-Valley-Coupling-Induced Large Spin-Lifetime Anisotropy in Bilayer Graphene. *Phys. Rev. Lett.* **2018**, *121*, 127702.
- (90) Vecera, P.; Edelthalhammer, K.; Hauke, F.; Hirsch, A. Reductive Arylation of Graphene: Insights Into a Reversible Carbon Allotrope Functionalization Reaction. *Phys. Status Solidi B* **2014**, *251*, 2536–2540.
- (91) Vecera, P.; Chacón-Torres, J. C.; Pichler, T.; Reich, S.; Soni, H. R.; Görling, A.; Edelthalhammer, K.; Peterlik, H.; Hauke, F.; Hirsch, A. Precise Determination of Graphene Functionalization by *In Situ* Raman Spectroscopy. *Nature Communications* **2017**, *8*, 15192.
- (92) Greenwood, N. N.; Earnshaw, A. *Chemistry of the Elements*; Butterworth: London, UK, 1998.
- (93) Basu, S.; Zeller, C.; Flanders, P. J.; Fuerst, C. D.; Johnson, W. D.; Fischer, J. E. Synthesis and Properties of Lithium–Graphite Intercalation Compounds. *Mater. Sci. Eng.* **1979**, *38*, 275–283.
- (94) Bergstrom, F. W.; Fernelius, W. C. The Chemistry of the Alkali Amides. *Chem. Rev.* **1933**, *12*, 43–179.
- (95) Juza, R. Amide der Alkali- und Erdalkalimetalle. *Angew. Chem.* **1964**, *76*, 290–300.

- (96) Cunningham, P. T.; Maroni, V. A. Laser Raman Spectra of Solid and Molten NaNH_2 : Evidence for Hindered Rotation of the NH_2^{-1} Ion. *J. Chem. Phys.* **1972**, *57*, 1415–1418.
- (97) Liu, A.; Song, Y. *In Situ* High-Pressure Study of Sodium Amide by Raman and Infrared Spectroscopies. *J. Phys. Chem. B* **2011**, *115*, 7–13.
- (98) Márkus, B. G.; Szirmai, P.; Kollarics, S.; Náfrádi, B.; Forró, L.; Chacón-Torres, J. C.; Pichler, T.; Simon, F. Improved Alkali Intercalation of Carbonaceous Materials in Ammonia Solution. *Phys. Status Solidi B* **2019**, *256*, 1900324.
- (99) Nemanich, R. J.; Solin, S. A.; Gerard, D. Raman Scattering from Intercalated Donor Compounds of Graphite. *Phys. Rev. B* **1977**, *16*, 2965–2972.
- (100) Fábíán, G.; Kramberger, C.; Friedrich, A.; Simon, F.; Pichler, T. A Broadband and High Throughput Single-Monochromator Raman Spectrometer: Application for Single-Wall Carbon Nanotubes. *Rev. Sci. Instrum.* **2011**, *82*.
- (101) Fábíán, G.; Kramberger, C.; Friedrich, A.; Simon, F.; Pichler, T. Adaptation of a Commercial Raman Spectrometer for Multiline and Broadband Laser Operation. *Phys. Status Solidi B* **2011**, *248*, 2581–2584.
- (102) Szirmai, P.; Fábíán, G.; Dóra, B.; Koltai, J.; Zólyomi, V.; Kürti, J.; Nemes, N. M.; Forró, L.; Simon, F. Density of States Deduced from ESR Measurements on Low-Dimensional Nanostructures; Benchmarks to Identify the ESR Signals of Graphene and SWCNTs. *Phys. Status Solidi B* **2011**, *248*, 2688–2691.
- (103) Saitta, A. M.; Lazzeri, M.; Calandra, M.; Mauri, F. Giant Nonadiabatic Effects in Layer Metals: Raman Spectra of Intercalated Graphite Explained. *Phys. Rev. Lett.* **2008**, *100*, 226401.
- (104) Chacón-Torres, J.; Dzsaber, S.; Vega-Díaz, S.; Akbarzadeh, J.; Peterlik, H.; Kottakoski, J.; Argentero, G.; Meyer, J.; Pichler, T.; Simon, F.; Terrones, M.; Reich, S. Potassium Intercalated Multiwalled Carbon Nanotubes. *Carbon* **2016**, *105*.